Geophysical Research Letters

RESEARCH LETTER
10.1029/2022GL102342

Key Points:

- Summer rainfall extremes over both central-eastern Tibetan Plateau (CETP) and Sichuan Basin (SCB) are dominated by the combination of eastward extended SAH and westward extended Western North Pacific Subtropical High
- The summer rainfall extremes over SCB are mainly induced by a low-level vortex imbedded in the background of large-scale circulations
- The dominant synoptic patterns over CETP and SCB all contribute to the increasing trends of frequency and intensity of the summer regional hourly EP events

Supporting Information:

Supporting Information may be found in the online version of this article.

Correspondence to:

A. Huang and D. Huang,
anhuang@nju.edu.cn;
huangdq@nju.edu.cn

Citation:

Xu, X., Huang, A., Huang, D., Zhang, Y., Gu, C., Cai, S., et al. (2023). What are the dominant synoptic patterns leading to the summer regional hourly extreme precipitation events over central-eastern Tibetan Plateau and Sichuan Basin? *Geophysical Research Letters*, *50*, e2022GL102342. https://doi.org/10.1029/2022GL102342

Received 1 DEC 2022
Accepted 16 FEB 2023

Author Contributions:

Conceptualization: Anning Huang
Data curation: Xiaoke Xu, Yong Tang
Formal analysis: Xiaoke Xu, Anning Huang, Danqing Huang

What Are the Dominant Synoptic Patterns Leading to the Summer Regional Hourly Extreme Precipitation Events Over Central-Eastern Tibetan Plateau and Sichuan Basin?

Xiaoke Xu[1], Anning Huang[1], Danqing Huang[1], Yan Zhang[2], Chunlei Gu[1], Shuxin Cai[1], Yong Tang[1], Zhizhan Zhao[1], and Jingwen Zeng[1]

[1]CMA-NJU Joint Laboratory for Climate Prediction Studies, School of Atmospheric Sciences, Frontiers Science Center for Critical Earth Material Cycling, Nanjing University, Nanjing, China, [2]Key Laboratory of Radiometric Calibration and Validation for Environmental Satellites, National Satellite Meteorological Center, China Meteorological Administration (LRCVES/CMA), FengYun Meteorological Satellite Innovation Center (FY-MSIC), Beijing, China

Abstract Revealing the synoptic patterns related to hourly extreme precipitation (EP) is very important to deepen our recognition and understanding of EP formation. The predominant synoptic patterns associated with the summer regional hourly EP events (RHEPE) over the central-eastern Tibetan Plateau (CETP) and Sichuan Basin (SCB) have been systematically identified. Results show the summer RHEPE over CETP and SCB are dominated by the background large-scale circulations featured by the configuration of eastward-extended South Asia high (SAH) and westward-extended Western North Pacific Subtropical High (WNPSH) and their northward advance, except for that an obvious low-level vortex imbedded in the background large-scale circulations is mainly responsible for the summer RHEPE over SCB. The frequency and intensity of the total summer RHEPE over CETP and SCB all show an obvious increasing trend during 2000–2020, which is largely contributed by the synoptic pattern characterized by the configuration of eastward extended SAH and westward extended WNPSH.

Plain Language Summary To completely indicate the synoptic patterns leading to the summer regional hourly extreme precipitation events (RHEPE) over the central-eastern Tibetan Plateau (CETP) and Sichuan Basin (SCB), this study has identified the dominant synoptic patterns of summer RHEPE over the two regions. Results show that the configuration of eastward extended South Asia high (SAH) and westward extended Western North Pacific Subtropical High (WNPSH) and their northward advance dominates the prime circulation patterns of summer RHEPE over CETP and SCB. However, in addition to the opposing motion of the SAH and WNPSH, a low-level vortex imbedded in the background large-scale circulations is mainly responsible for the summer RHEPE over SCB. The findings of this study may help us to deepen our understanding of the RHEPE formation over the two regions with complex terrain and provide a base to further improve the prediction of extreme precipitation.

1. Introduction

Extreme precipitation (EP) is the main cause of floods, urban waterlogging, debris flow, and soil erosion, which threaten the safety of millions of people life and the development of the economy (Nie & Sun, 2021; Tang et al., 2021; Zou & Ren, 2015). In recent years, the intensity and frequency of EP have significantly increased in most parts of China (Ng et al., 2021; Tang et al., 2021; Zhao et al., 2020). However, as a key region of intense land-atmosphere interaction, water cycle, and energy balance, the EP over Tibetan Plateau (TP) and adjacent areas have been rarely studied due to sparse observation (Chen, 2022; Luo et al., 2016; Xiao et al., 2016).

In September 2011, an EP induced the outburst of Zonag lake, which caused the flood and the interception of the migration path of lambing over the south of the lake (Pei et al., 2019). Moreover, during 11–20 August 2020, an EP in Sichuan province directly engendered suffering for 8.523 million people, among which 58 sadly died and 13 were recorded as missing (Qian et al., 2022). The regional EP with much larger coverage than the local EP brings serious disaster (Ng et al., 2021). Consequently, revealing the generation/development mechanism of regional EP and improving its prediction/risk-evaluation ability are crucial for ecological and environmental protection, water resource utilization, and climate change adaptation (Tang et al., 2021; Zhao et al., 2020).

Investigation: Xiaoke Xu, Anning Huang, Yan Zhang, Chunlei Gu, Shuxin Cai, Zhizhan Zhao, Jingwen Zeng
Methodology: Xiaoke Xu, Anning Huang
Resources: Xiaoke Xu, Anning Huang, Yan Zhang, Jingwen Zeng
Software: Xiaoke Xu, Yong Tang, Jingwen Zeng
Supervision: Anning Huang
Validation: Xiaoke Xu, Anning Huang, Danqing Huang
Visualization: Xiaoke Xu, Chunlei Gu
Writing – original draft: Xiaoke Xu, Anning Huang
Writing – review & editing: Xiaoke Xu, Anning Huang, Danqing Huang, Yan Zhang, Chunlei Gu, Shuxin Cai, Yong Tang, Zhizhan Zhao

The EP over Central-eastern Tibetan Plateau (CETP) and Sichuan Basin (SCB) in summer significantly shows a diurnal variation, it begins in afternoon (early evening) and peaks in early evening (midnight) (Li, 2018; Zhao et al., 2020). Hence, the intensity and amount of EP over the CETP and SCB are stronger at night than in daytime (Li, 2018; Zheng et al., 2019). In addition, the duration of EP events over CETP and SCB in summer is less than 10 hr (Li, 2018; Li et al., 2013). Naturally, it needs observation data with much higher resolutions of time and space to reveal the detailed features of EP.

In recent years, global warming has further exacerbated the frequency and intensity of EP following the Clausius-Clapeyron relation (Trenberth, 1998). Particularly, the hourly EP is more susceptible to surface temperature and moisture-holding capacity of the atmosphere than the daily and sub-daily scale ($3 < t < 24$ hr) (Chen et al., 2021; Park & Min, 2017; Tang et al., 2020; Wu & Luo, 2019). The hydrometeorological and geologic hazards induced by the EP at hourly timescale are different from those at daily scale (Zhao et al., 2020). The hourly EP data can capture the elaborate features in the process of EP events (such as the duration and diurnal variation) (Li, 2018; Li et al., 2013; Zhao et al., 2020). Obviously, using the hourly precipitation and reanalysis data to identify the predominant circulation systems of regional hourly EP events (RHEPE) over TP and SCB is necessary.

There are still evident challenges in describing, modeling, and forecasting the process of EP at hourly or sub-daily time scale (Pfahl et al., 2017; Zhang et al., 2017). For promoting the prediction of EP, researchers have developed and improved numerical models and prediction technology (such as increasing model resolution and improving the parameterization schemes) (Huang et al., 2020; Tian et al., 2020; Zhong & Yang, 2015), and explored the machine learning utilized in EP (such as cluster analysis and the attribution simulations based on circulation similarity) (Qian et al., 2022; Tang et al., 2021; Ye & Qian, 2021).

Identifying the synoptic weather patterns based on the machine learning method is an effective way to understand the occurrence mechanism of EP (Utsumi et al., 2016, 2017). The EP over the TP and SCB in summer may be influenced by various-scale synoptic systems, such as the Indian monsoon, East Asian monsoon, the mid-latitude westerlies, and the local moisture recycling (Bolch et al., 2012; Duan et al., 2011; Tian et al., 2007; Xu et al., 2008; Yao et al., 2012). There are many vital factors affecting the generation and development of EP, such as the strength of monsoon (Yao et al., 2012; Zhu et al., 2015), the movement of western North Pacific Subtropical High (WNPSH) and South Asia High (SAH) (Liu et al., 2016; Nie & Sun, 2021), anomalous lows over TP (Bin & Xiang, 2016; Nie & Sun, 2021; Qian et al., 2015), and the path of water vapor transportation (Hu et al., 2015; Liu et al., 2016; Xia et al., 2021). Previous studies pointed out the low vortex/shear line pattern is the main synoptic pattern over SCB (Luo et al., 2016; Wu & Luo, 2019). The collaborative impacts of the multiple systems at different levels on the RHEPE are not well revealed. Meanwhile, there are few researches exploring the dominant synoptic patterns of RHEPE over TP and adjacent areas.

Compared to the previous case studies, we uncover the configuration of the synoptic systems at different levels responsible for the summer RHEPE over CETP and SCB from a climatic perspective, which may provide the universality of atmospheric conditions related to RHEPE. In this study, we mainly focus on addressing the following two questions: What are the spatial-temporal characteristics of the summer RHEPE over CETP and SCB in the recent 21 years? What are the typical synoptic patterns leading to the summer RHEPE over CETP and SCB?

2. Data and Method

2.1. Data

The data used in study are listed as follows:

1. The latest version (V06) of the half-hourly Integrated Multi-satellite Retrievals for Global Precipitation Measurement (GPM-IMERG) with 0.1° resolution during 2000–2020 (Hou et al., 2014), which can well capture the precipitation spatial-temporal distribution over TP and SCB in summer (Ma et al., 2016; Tang et al., 2020; Yang et al., 2020; Zhang et al., 2018). The GPM-IMERG data in summer (June, July, and August) is converted into hourly precipitation for revealing the characteristics of summer RHEPE over the CETP and SCB.
2. The fifth generation of ECWMF atmospheric reanalysis data (ERA5) with a horizontal resolution of 0.25° and temporal resolution of 1 hr over the period of 2000–2020 (Hersbach et al., 2020), which has high confidence in the precision over the TP and SCB (Sun et al., 2021; Xia et al., 2021).
3. The Shuttle Radar Topography Mission (SRTM) Digital Elevation Database v4.1 with the horizontal resolution of 3 arc s (~90 m) (Jarvis et al., 2008).

2.2. Definition of Extreme Precipitation and Regional Events

The 95th percentile of all historical hourly precipitation records with an intensity ≥0.1 mm in the summers of 2000–2020 is regarded as the EP threshold at each grid (He & Zhai, 2018; Xie et al., 2018). The EP for each grid at a given time is detected when the precipitation intensity exceeds the 95th percentile threshold. The 95th percentile of grid numbers (≥1) with simultaneous EP over a given region in the summers of 2000–2020 is taken as the RHEPE threshold (Tang et al., 2021). And then we can detect the RHEPE when the number of grids with simultaneous EP exceeds the 95th percentile threshold of the counted grid numbers within a specific region at a given time. For some RHEPEs that have the same number of grids with simultaneous EP but different distributions, we regard them as separate events. We detected 2334 (2330) RHEPE in the summers of 2000–2020 over CETP (SCB).

2.3. Definition of South Asia High, Western North Pacific Subtropical High, and Low-Level Vortex

The 1,255 dagpm contour at 200 hPa is taken as the reference line of South Asia High (SAH) (Wu et al., 2015). The 586 dagpm contour at 500 hPa is taken as the reference line of the Western North Pacific Subtropical High (WNPSH) (Wei et al., 2014). The low-level vortex over SCB is represented by the closed 144 dagpm contour at 850 hPa (Mu & Li, 2017).

2.4. Method

Based on the SRTM terrain height data, the sub-grid topography standard deviation (Sd) reflecting the terrain complexity within a given grid(i, j) of the 0.1° GPM data is calculated by Wu et al. (2018):

$$Sd = \sqrt{\frac{1}{14641}\sum_{i1=ii-60}^{i1=ii+60}\sum_{j1=jj-60}^{j1=jj+60}\left(h_{i1,j1}-\overline{h}\right)^2} \quad (1)$$

$$\overline{h} = \frac{1}{14641}\sum_{i1=ii-60}^{i1=ii+60}\sum_{j1=jj-60}^{j1=jj+60}\left(h_{i1,j1}-\overline{h}\right)^2 \quad (2)$$

where $\overline{h}$ represents the regional mean terrain height of the 14,641 (121 × 121) sub-grid points within a grid of 0.1° by 0.1°. $h(i1, j1)$ is the sub-grid terrain height of SRTM. The $i1$ and $j1$ indicate the sub-grid number centered by the sub-grid (ii, jj) for the west-east direction and south-north direction, respectively. The sub-grid numbers ii and jj were converted from the grid numbers i and j based on the relation between sub-grids (3 arc s) and GPM grids (0.1°), respectively.

Mann-Kendall method (Gilbert, 1987; Kendall, 1975; Mann, 1945) is used to evaluate the statistical significance of temporal trends for the frequency and intensity of RHEPE.

2.5. Clustering Method

Compared with the K-means method, spectral clustering has stronger adaptability to data distribution, a better clustering effect, and less computation (von Luxburg, 2007). It performs traditional clustering on affinity matrix rather than raw data and is rarely applied in atmospheric science yet (Tang et al., 2021). This study adopted the python machine learning package (Pedregosa et al., 2011) containing spectral clustering to conduct cluster analysis on the wind fields at 500 , 300, and 200 hPa levels for CETP (925 , 850, 700, 500, and 200 hPa levels for SCB) when the RHEPE happens. u and v wind components on each grid point are reduced to a time-only array and normalized time series. Some options in the algorithm need to be set before calculating, such as setting the "nearest_neighbors" to construct the affinity matrix and the "kmeans" is selected to assign the cluster labels. Finally, the classification cluster sequence corresponding to the time series is obtained for synoptic pattern analysis.

3. Result

3.1. Background

The altitude decreased from northwest to southeast over TP with much larger topographic fluctuation in southeastern TP (Figures 1a and 1b). Topography uplifts the airflow, blocks the synoptic systems and water vapor transportation and further affects the amount, intensity, frequency, and duration of EP (Hu et al., 2021; Sandvik

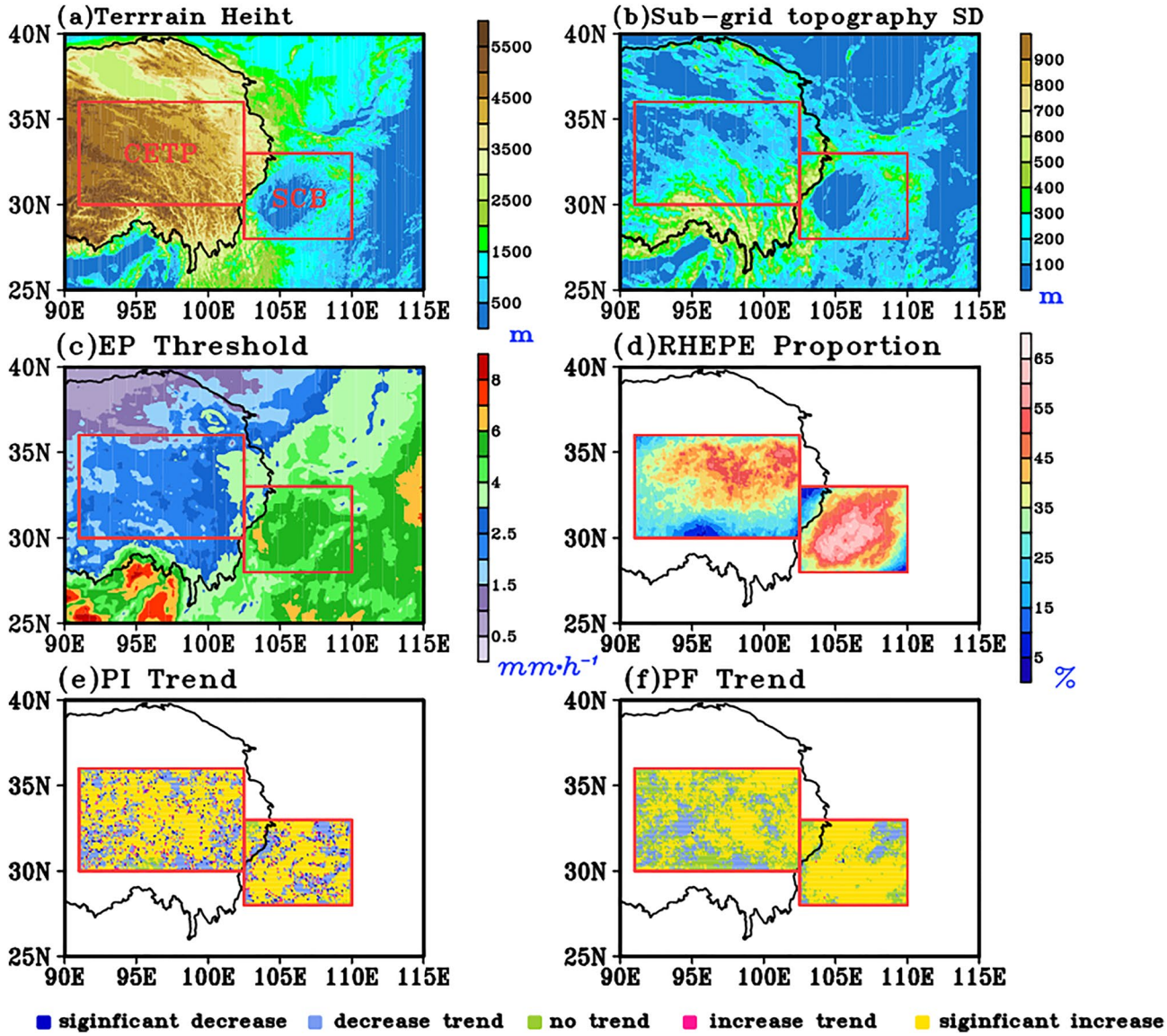

Figure 1. The distribution of terrain height (a), sub-grid topographic standard deviation (b), and the sub-region boundaries (red box) for CETP and SCB. The distribution of the EP threshold in summers of 2000–2020 based on the 95th percentile is shown in (c). The contribution of EP amount in RHEPE to the total EP is presented in (d). The distribution of trends of EP intensity and frequency when RHEPE happens over CETP and SCB during 2000–2020 is shown in (e and f), respectively. The statistical significance of trends is tested by the Mann-Kendall method, and the significant increase/decrease trend is at the 0.05 significance level.

et al., 2018; Shen et al., 2022). Based on the similar topographic fluctuation and comparable EP threshold, we focus on the two sub-regions: CETP (30°N–36°N, 90.5°E–102.5°E) and SCB (28°N–33°N, 102.5°E–110°E) (Figures 1b and 1c). The EP amount during the RHEPE over the CETP (SCB) contributes more than 45.6% (55.2%) of the total EP amount on the regional average therein with much larger contributions over north CETP (central SCB) (Figure 1d). Meanwhile, the intensity and frequency of the RHEPE over most parts of CETP and SCB show significant increasing trends during 2000–2020 (Figures 1e and 1f).

3.2. Synoptic Patterns Responsible for the Summer RHEPE Over CETP

3.2.1. The Features of Synoptic Patterns

Cluster analysis identifies two (cluster numbers are referenced by an objective score according to Caliński & Harabasz, 1974) synoptic patterns responsible for the summer RHEPE over CETP (Figure 2). The synoptic

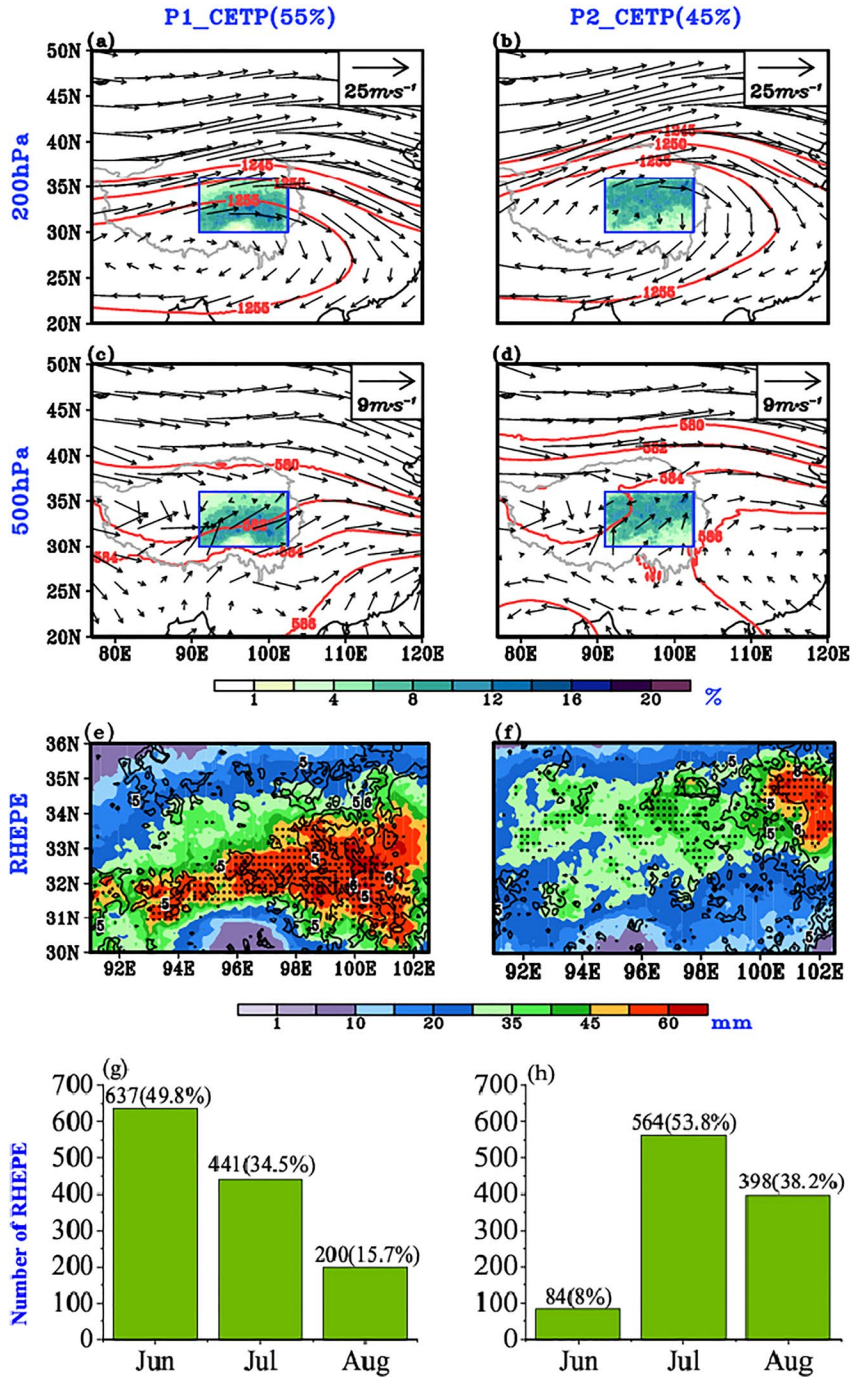

Figure 2. The synoptic patterns responsible for the summer RHEPE over CETP revealed by clustering at 200 hPa (a–b) and 500 hPa (c–d). The mean wind field (vector, units: ms^{-1}), geopotential heights (contour, units: dagpm), and occurrence probability of EP (shaded, units: %) under each synoptic pattern are shown in (a–d). (e, f) show the distribution of occurrence probability of EP (grids with the EP occurrence probability greater than 10% are dotted), intensity (contour, units: mm h^{-1}), and amount (shaded, units: mm) of RHEPE under different synoptic patterns over CETP. (g, h) show the RHEPE occurrences (units: hour) under different synoptic patterns in June, July, and August with the contributions (numbers in the brackets, units: %) to the total RHEPE occurrence in summer during 2000–2020.

pattern 1 leading to 55% of the total RHEPE occurrences is characterized by the SAH at 200 hPa covering southern TP (Figure 2a) with the WNPSH at 500 hPa located south accompanied by the southwesterly wind over CETP (Figure 2c). Under this synoptic pattern, relatively higher EP occurrence probability, which is defined

as the ratio of total EP occurrences at each grid under a given synoptic pattern to the total occurrences of this synoptic pattern (Tang et al., 2021), mainly concentrates in the southeast CETP (Figures 2a and 2c). The maximal cumulative rainfall amount induced by the RHEPE in summer averaged over 2000–2020 with the intensity above 60 mm and maximal EP intensity above 6 mm hr^{-1} are mainly located over the southeast CETP (Figure 2e), this is well corresponding to the location of the high EP occurrence probability. The synoptic pattern 1 predominantly occurs in June and July with a portion of 84.3% (Figure 2g), this is consistent with the principle that the WNPSH is located farther south in June and July than in August (Xu et al., 2020).

The synoptic pattern 2 results in 45% of the total RHEPE occurrence in summer over CETP, it is featured by the northward advance of strengthened SAH at the 200 hPa covering the whole CETP (Figure 2b) and intensified and northwestward extended WNPSH with prevailing southwesterly winds at 500 hPa over CETP (Figure 2d) compared to the synoptic pattern 1 (Figures 2a and 2c). Under this synoptic pattern, relatively higher EP occurrence probability is mainly located in the northeast CETP, where the maximum cumulative EP amount induced by the RHEPE with a magnitude of ∼50 mm and maximal EP intensity of 6 mm hr^{-1} are located (Figure 2f). The synoptic pattern 2 of summer RHEPE over CETP frequently occurs in July and August with a portion of 92% (Figure 2h), corresponding well to the farther north location of the WNPSH relative to the synoptic pattern 1.

In addition, the frequency and regionally mean intensity of the total summer RHEPE over CETP all show an obvious increasing trend during the recent two decades with much more significant increasing trend of intensity (Figures S1b and S1d in Supporting Information S1). And both the synoptic patterns all contribute to the increasing trends in the frequency and intensity of total RHEPE, except that the trends are relatively larger under the synoptic pattern 1 than under the synoptic pattern 2 (Figure S1e in Supporting Information S1).

3.2.2. Impact of the Synoptic Patterns on the Summer RHEPE Over CETP

How the different synoptic systems affect the summer RHEPE over CETP will be addressed in the following section. As shown in Figure 3a, the synoptic pattern 1 for the summer RHEPE over CETP is characterized by the eastward extended SAH and westward extended WNPSH with the strengthened southwesterly water vapor transport. From Figure 3c, the anomalous divergence at 200 hPa and anomalous convergence at 500 hPa under the synoptic pattern 1 is helpful to strengthen the upward motion over the south CETP and thereafter induced EP occurrence (Figures 2a and 2c) there (Figure 2e).

Compared to the synoptic pattern 1, both the strengthened SAH with eastward extension and the intensified WNPSH with westward extension are located farther north with strengthened southeasterly water vapor transport under the synoptic pattern 2 (Figure 3b). Meanwhile, from Figures 3c and 3d, the anomalous convergence (divergence) at 500 hPa (200 hPa) under the synoptic pattern 2 favors intensifying the upward motion over the north CETP and thereafter much larger EP occurrence probability (Figures 2b and 2d) and more rainfall there (Figure 2f).

From the evolution of the atmospheric conditions at different levels during the 12–0 hr before the RHEPE occurrence under both synoptic patterns (Figure S2 in Supporting Information S1), the SAH at 200 hPa clearly exhibits a gradual strengthening process, the WNPSH at 500 hPa is stable before the RHEPE occurrence.

Overall, the upward motion and water vapor transportation strongly vary with the configurations of the SAH and WNPSH under different synoptic patterns of the summer RHEPE and determine the location and magnitude of EP over CETP. Particularly, the variation of SAH before the RHEPE occurrence maybe an important signal for the prediction of RHEPE.

3.3. Synoptic Patterns Responsible for the Summer RHEPE Over SCB

3.3.1. The Features of Synoptic Patterns

The typical synoptic patterns related to the summer RHEPE over SCB can be divided into twocategories (Figure 4). The synoptic pattern 1 leading to 52.6% of the total RHEPE occurrences is featured by the SAH at 200 hPa covering the entire SCB with the WNPSH at 500 hPa extending westward to the southeast SCB (Figures 4a and 4c). Meanwhile, an evident low-level vortex at 850 hPa is located in the western SCB with southerly wind prevailing there (Figure 4e). Under this synoptic pattern, the relatively higher EP occurrence probability is mainly distributed in the southwest SCB, where the accumulated EP amount is more than 200 mm in summer averaged over 2000–2020 with a maximal EP intensity center of 11 mm hr^{-1} (Figure 4g). Associated

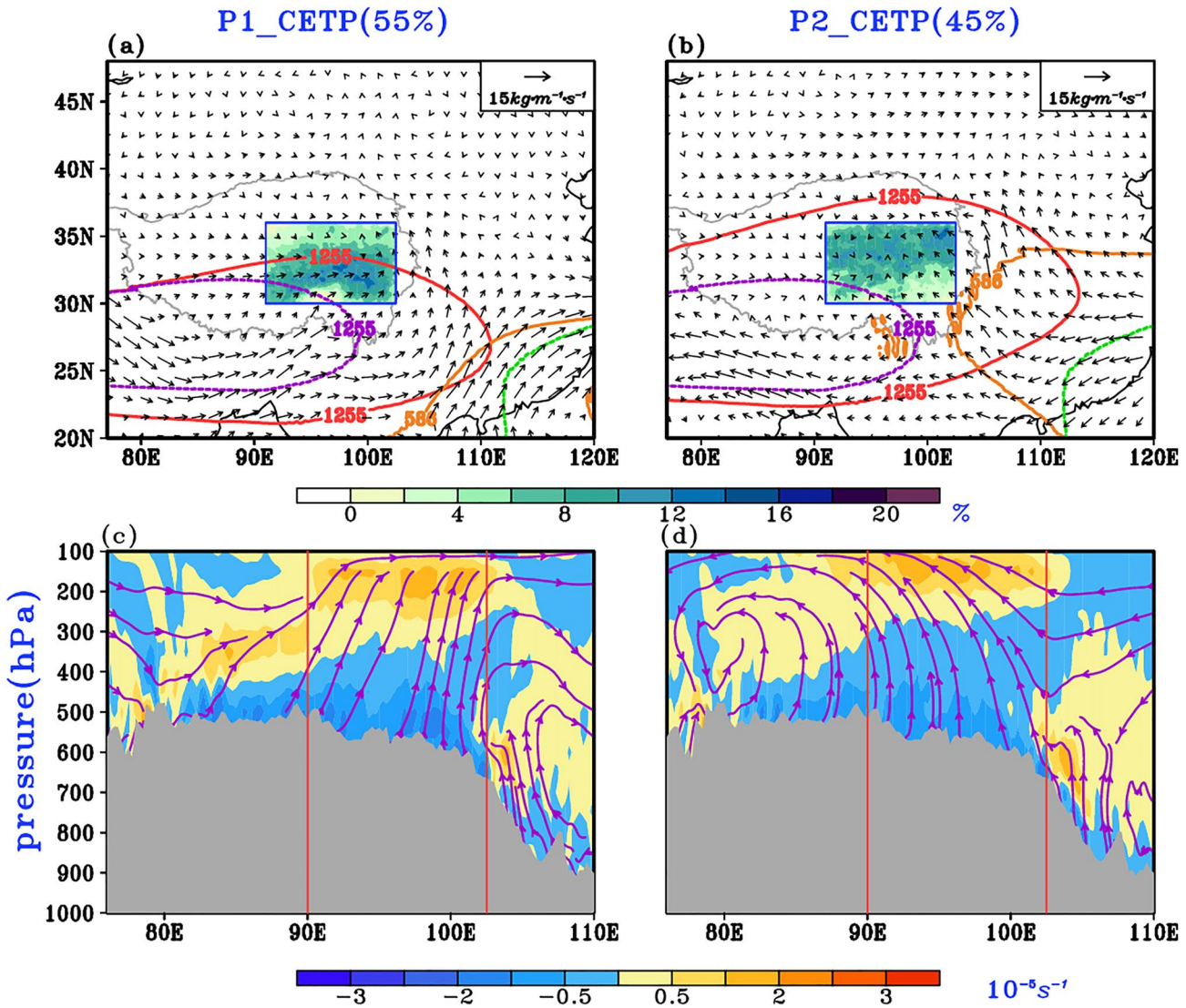

Figure 3. Configuration of South Asian High (SAH) (climatology: purple dotted lines, synoptic pattern: red solid lines, units: dagpm) and Western North Pacific Subtropical High (WNPSH) (climatology: green dotted lines, synoptic pattern: orange solid lines, units: dagpm) with the occurrence probability of EP (shaded) and the anomalous water vapor transport flux vertically integrated from surface to 300 hPa (vector, units: kg m^{-1} s^{-1}) during RHEPE under each synoptic pattern over CETP (a–b). The pressure-longitude cross-section of anomalous convergence (shaded) and atmospheric circulation (stream) averaged along 31°N to 35°N under each synoptic pattern in summer relative to the climatology of 2000–2020 (c–d). The gray shadings in (c, d) show the terrain height.

with the northward movement of WNPSH, the summer RHEPE over SCB under the synoptic pattern 1 mainly occurs in July and August with a portion of 86.5% (Figure 4i).

The other synoptic pattern responsible for the summer RHEPE over SCB accounts for 47.4% of the total RHEPE occurrences. The synoptic pattern is mainly featured by the westward retreat of SAH at 200 hPa compared to the synoptic pattern 1 (Figures 4b and 2b) with a shallow trough located in the southwestern SCB at 500 hPa (Figure 4d). The low-level vortex is located in central SCB with the strong southwesterly wind bringing abundant water vapor (Figure 4f). Under this pattern, a much higher EP occurrence probability and more rainfall (Figure 4h) are located in the southeastern SCB. Relative to synoptic pattern 1, as the WNPSH is located farther south, the synoptic pattern 2 mainly occurs in June (Figure 4j).

Meanwhile, the frequency and regional mean intensity of the total RHEPE in summer over SCB all show an obvious increasing trend in the recent two decades with much more significant increasing trend in intensity (Figures S1b and S1d in Supporting Information S1), this is similar to the situation in CETP (Figures S1a and S1c in Supporting Information S1). Furthermore, both the synoptic patterns all contribute to the increasing trends in the

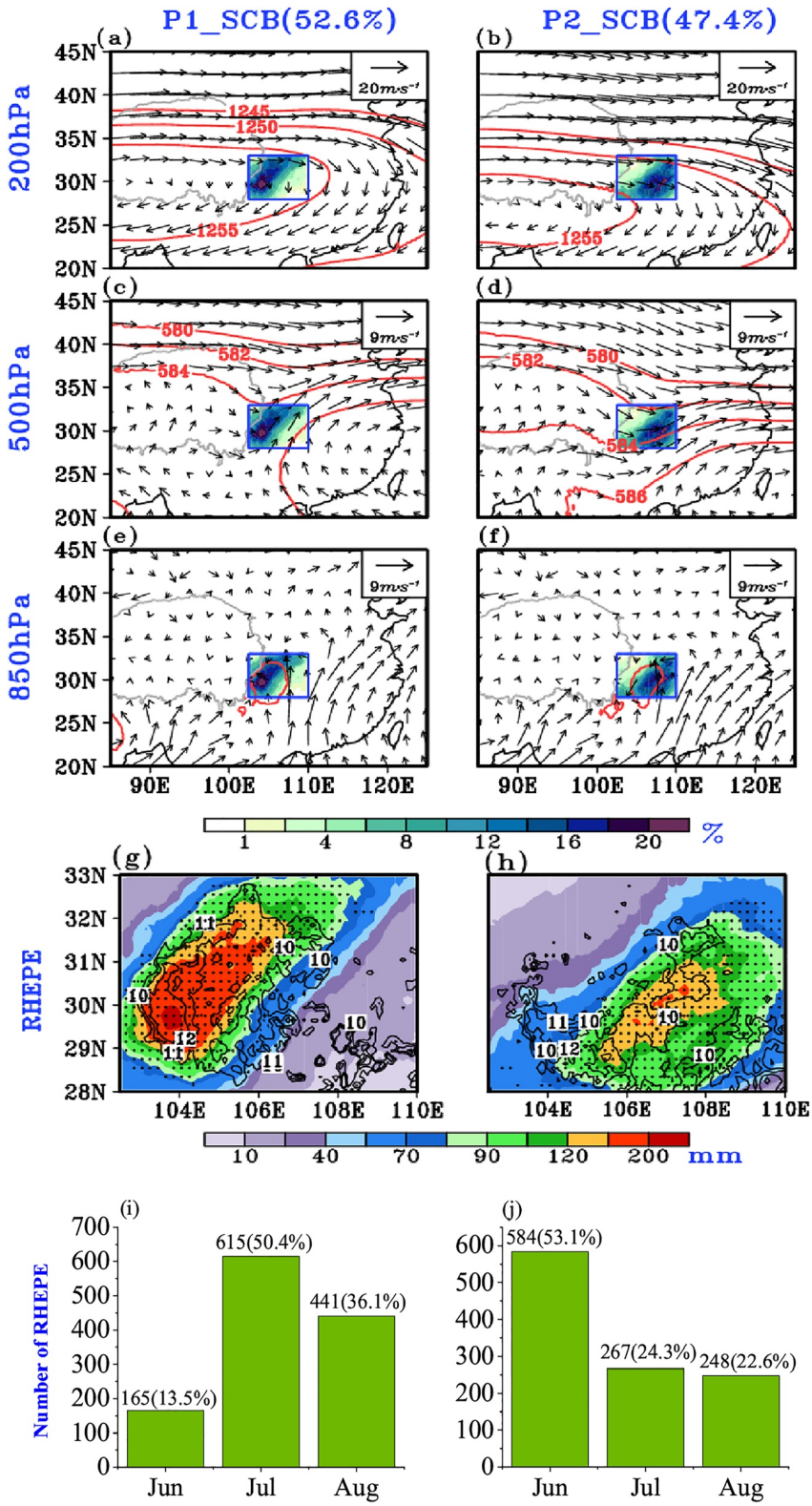

Figure 4. The synoptic patterns responsible for the summer RHEPE over SCB revealed by clustering at 200 hPa (a–b), 500 hPa (c–d), and 850 hPa (e–f). The mean wind fields (vector, units: m s^{-1}), geopotential heights (contour, units: dagpm), and occurrence probability of EP (shaded, units: %) under each synoptic pattern are shown in (a–f). (g, h) show the distribution of occurrence probability of EP (grids with the EP occurrence probability greater than 10% are dotted), EP intensity (contour, units: mm h^{-1}), and EP amount (shaded, units: mm) during RHEPE under each synoptic pattern over SCB. (i, j) show the RHEPE occurrences (units: hour) under each synoptic pattern in June, July, and August with the contributions (numbers in the brackets, units: %) to the total RHEPE occurrences in summer during 2000–2020.

frequency and intensity of total RHEPE, except that the trends are relatively larger under synoptic pattern 2 than under synoptic pattern 1 (Figure S1e in Supporting Information S1).

3.3.2. Impact of the Synoptic Patterns on the Summer RHEPE Over SCB

Under the synoptic pattern 1, relative to the climatology, the much stronger and westward extended SAH and the relatively stronger WNPSH with northwestward extension overlap together with strengthened southerly water transport over the southeast SCB and a low-level vortex over west SCB (Figure 5a). Meanwhile, the anomalous convergence induced by the low-level vortex and the anomalous divergence caused by the strengthened SAH favor the upward motion over southwest SCB (Figure 5c) and thereafter much higher EP occurrence probability (Figure 5a) and more rainfall (Figure 4g) therein.

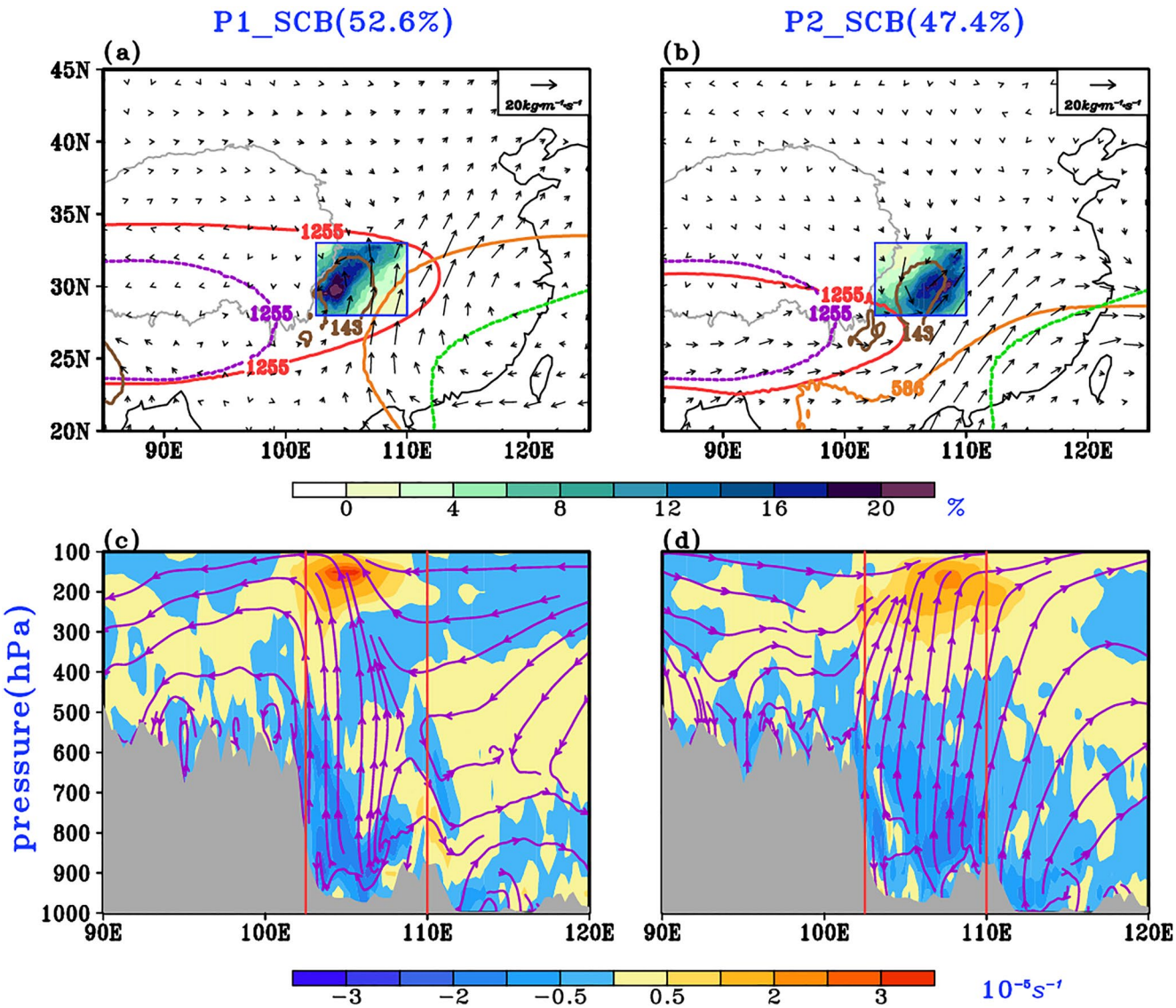

Figure 5. Configuration of South Asian High (SAH) at 500 hPa (climatology: purple dotted lines, synoptic pattern: red solid lines, units: dagpm), Western North Pacific Subtropical High (WNPSH) at 200 hPa (climatology: green dotted lines, synoptic pattern: orange solid lines, units: dagpm) and the low vortex at 850 hPa indicated by a closed contour of 143 dagpm geopotential height with the occurrence probability of EP (shaded, units: %) and the anomalous water vapor transport flux vertically integrated from surface to 300 hPa (vector, units: kg m^{-1} s^{-1}) during RHEPE under each synoptic pattern over SCB (a, b). The pressure-longitude cross-section of anomalous convergence (shaded) and atmospheric circulation (stream) under each synoptic pattern averaged along 29°N to 32°N in summer relative to the climatology of 2000–2020 (c, d). The gray shadings in (c, d) represent the terrain height.

Compared to the synoptic pattern 1, synoptic pattern 2 of summer RHEPE over SCB is featured by the southward retreat of weakened SAH and WNPSH with a low-level vortex located in central-eastern SCB and southwesterly water vapor transport anomalies (Figure 5b). Correspondingly, the anomalous upward motion shifts eastward (Figure 5d) with the strengthened southwesterly water vapor transport (Figure 5b) along eastern SCB, where the EP occurrence probability (Figure 5b) and the rainfall induced by the RHEPE (Figure 4h) are much higher.

From the evolution of the atmospheric conditions at different levels before the RHEPE occurrence, the SAH under synoptic pattern 1 exhibits a westward shift, as well as slight variations in the position of the WNPSH and low vortex (Figure S3 in Supporting Information S1). However, the SAH, WNPSH, and low vortex under synoptic pattern 2 have no apparent changes during the 12 hr before the RHEPE occurrence (Figure S3 in Supporting Information S1).

Overall, an obvious low-level vortex imbedded in the eastward extended SAH with westward extended WNPSH is a mainly synoptic feature for the summer RHEPE over SCB. Similarly, the evaluation of SAH before the RHEPE occurrence maybe an important signal for the prediction of RHEPE.

4. Summary and Discussion

The hourly satellite retrieved precipitation and reanalysis data are used to identify the predominant synoptic patterns related to the RHEPE in the summers of 2000–2020 over CETP and SCB. Results show that the frequency and intensity of summer rainfall extremes when RHEPE happens over CETP and SCB exhibit significant increasing trends in the recent two decades. The summer RHEPE over both CETP and SCB are dominated by the background large-scale circulations featured by the configuration of the eastward extended SAH and westward extended WNPSH, which largely contributes to the increasing trends in the frequency and intensity of total RHEPE in summer during 2000–2020. In particular, the summer RHEPE over SCB is mainly induced by a low-level vortex imbedded in the background of large-scale circulations. The water vapor transportation determined by the different predominant synoptic patterns leads to the significant diversity of RHEPE over CETP and SCB in summer.

The summer RHEPE over both CETP and SCB are influenced by the combination of eastward extension of SAH and westward extension of WNPSH, but the amount, frequency, and intensity of RHEPE over these two regions have striking differences. It is non-negligible that the terrain affects the RHEPE over CETP and SCB (Chow & Chan, 2009; Ma et al., 2018; Tuel & Martius, 2022). Although this study revealed the configuration of multiple climate systems, the quantitative impact of topography needs to be further investigated through numerical experiments in the future.

Data Availability Statement

The GPM-IMERG precipitation data can be downloaded from https://disc.gsfc.nasa.gov/datasets/GPM_3IMERGDF_06/summary/. The ERA5 reanalysis data are available from https://cds.climate.copernicus.eu/cdsapp#!/search?type=dataset. The Shuttle Radar Topography Mission (SRTM) 90m Digital Elevation Database v4.1 was used in this study, which is available at https://developers.google.com/earth-engine/datasets/catalog/CGIAR_SRTM90_V4.

Acknowledgments
This study is founded by the National Key R&D Program of China under Grant 2022YFF0801601, the National Natural Science Foundation of China under Grants 41975081 and 42075020, CAS "Light of West China" Program (E12903010, Y929641001), the Research Funds for the Frontiers Science Center for Critical Earth Material Cycling Nanjing University, the Fundamental Research Funds for the Central Universities (020914380103, 020914380104), the Jiangsu University "Blue Project" outstanding young teachers training object, and the Jiangsu Collaborative Innovation Center for Climate Change. The authors show their deepest respect and warm appreciation to the editor and two anonymous reviewers for their constructive suggestions to greatly improve the manuscript.

References

Bin, C., & Xiang, D. X. (2016). Spatiotemporal structure of the moisture sources feeding heavy precipitation events over the Sichuan Basin. *International Journal of Climatology*, *36*(10), 3446–3457. https://doi.org/10.1002/joc.4567

Bolch, T., Kulkarni, A., Kääb, A., Huggel, C., Paul, F., Cogley, J. G., et al. (2012). The state and fate of Himalayan glaciers. *Science*, *336*(6079), 310–314. https://doi.org/10.1126/science.1215828

Caliński, T., & Harabasz, J. (1974). A dendrite method for cluster analysis. *Communicatio-n in Statistics–Theory and Methods*, 3(1), 1–27. https://doi.org/10.1080/03610927408827101

Chen, H. (2022). Key regions where land surface processes shape the East Asian climate. *Atmospheric and Oceanic Science Letters*, *15*(3), 100209. https://doi.org/10.1016/j.aosl.2022.100209

Chen, Y., Li, W., Jiang, X., Zhai, P., & Luo, Y. (2021). Detectable intensification of hourly and daily scale precipitation extremes across eastern China. *Journal of Climate*, *34*(3), 1185–1201. https://doi.org/10.1175/jcli-d-20-0462.1

Chow, K. C., & Chan, J. C. (2009). Diurnal variations of circulation and precipitation in the vicinity of the Tibetan Plateau in early summer. *Climate Dynamics*, *32*(1), 55–73. https://doi.org/10.1007/s00382-008-0374-x

Duan, A., Li, F., Wang, M., & Wu, G. (2011). Persistent weakening trend in the spring sensible heat source over the Tibetan Plateau and its impact on the Asian summer monsoon. *Journal of Climate*, *24*(21), 5671–5682. https://doi.org/10.1175/jcli-d-11-00052.1

Gilbert, R. O. (1987). *Statistical methods for environmental pollution monitoring*. Wiley.

He, B. R., & Zhai, P. M. (2018). Changes in persistent and non-persistent extreme precipitation in China from 1961 to 2016. *Advances in Climate Change Research*, *9*(3), 177–184. https://doi.org/10.1016/j.accre.2018.08.002

Hersbach, H., Bell, B., Berrisford, P., Hirahara, S., Horanyi, A., Munoz-Sabater, J., et al. (2020). The ERA5 global reanalysis. *Quarterly Journal of the Royal Meteorological Society*, *146*(730), 1999–2049. https://doi.org/10.1002/qj.3803

Hou, A. Y., Kakar, R. K., Neeck, S., Azarbarzin, A. A., Kummerow, C. D., Kojima, M., et al. (2014). The global precipitation measurement mission. *Bulletin of the American Meteorological Society*, *95*(5), 701–722. https://doi.org/10.1175/bams-d-13-00164.1

Hu, X., Yuan, W., & Yu, R. (2021). The extraordinary rainfall over the eastern Periphery of the Tibetan Plateau in August 2020. *Advances in Atmospheric Sciences*, *38*(12), 2097–2107. https://doi.org/10.1007/s00376-021-1134-7

Hu, Y., Zhai, P., Liu, L., Chen, Y., & Liu, Y. (2015). Dominant large-scale atmospheric circulation systems for the extreme precipitation over the western Sichuan Basin in summer 2013. *Advances in Meteorology*, *2015*, 1–10. https://doi.org/10.1155/2015/690363

Huang, Y., Wang, Y., Xue, L., Wei, X., Zhang, L., & Li, H. (2020). Comparison of three microphysics parameterization schemes in the WRF model for an extreme rainfall event in the coastal metropolitan City of Guangzhou, China. *Atmospheric Research*, *240*, 104939. https://doi.org/10.1016/j.atmosres.2020.104939

Jarvis, A., Reuter, H. I., Nelson, A., & Guevara, E. (2008). The Shuttle radar topography mission (SRTM) 90m digital elevation Database v4.1 [Dataset]. International Centre for Tropical Agriculture (CIAT). Retrieved from https://developers.google.com/earth-engine/datasets/catalog/CGIAR_SRTM90_V4

Kendall, M. G. (1975). *Rank correlation methods* (4th ed.). Charles Griffin.

Li, J. (2018). Hourly station-based precipitation characteristics over the Tibetan Plateau. *International Journal of Climatology*, *38*(3), 1560–1570. https://doi.org/10.1002/joc.5281

Li, J., Yu, R., & Sun, W. (2013). Duration and seasonality of hourly extreme rainfall in t-he central eastern China. *Acta Meteorologica Sinica*, *27*(6), 799–807. https://doi.org/10.1007/s13351-013-0604-y

Liu, W., Wang, L., Chen, D., Tu, K., Ruan, C., & Hu, Z. (2016). Large-scale circulation classification and its links to observed precipitation in the eastern and central Tibetan Plateau. *Climate Dynamics*, *46*(11), 3481–3497. https://doi.org/10.1007/s00382-015-2782-z

Luo, Y., Wu, M., Ren, F., Li, J., & Wong, W. K. (2016). Synoptic situations of extreme hourly precipitation over China. *Journal of Climate*, *29*(24), 8703–8719. https://doi.org/10.1175/jcli-d-16-0057.1

Ma, Y., Lu, M., Chen, H., Pan, M., & Hong, Y. (2018). Atmospheric moisture transport versus precipitation across the Tibetan Plateau: A mini-review and current challenges. *Atmospheric Research*, *209*, 50–58. https://doi.org/10.1016/j.atmosres.2018.03.015

Ma, Y., Tang, G., Long, D., Yong, B., Zhong, L., Wan, W., & Hong, Y. (2016). Similarity and error intercomparison of the GPM and its predecessor-TRMM multisatellite precipitation analysis using the best available hourly gauge network over the Tibetan Plateau. *Remote Sensing*, *8*(7), 569. https://doi.org/10.3390/rs8070569

Mann, H. B. (1945). Non-parametric tests against trend. *Econometrica*, *13*(3), 163–171. https://doi.org/10.2307/1907187

Mu, D., & Li, Y. Q. (2017). Statistical characteristics summary of the southwest China Vortex. *Journal of Arid Meteorology*, *02*(0175), 1006–7639. http://www.ghqx.org.cn/EN/Y2017/V35/I2/175

Ng, C. P., Zhang, Q., & Li, W. (2021). Changes in hourly extreme precipitation over eastern China from 1970 to 2019 dominated by synoptic-scale precipitation. *Geophysical Research Letters*, *48*(5), e2020GL090620. https://doi.org/10.1029/2020GL090620

Nie, Y., & Sun, J. (2021). Synoptic-scale circulation precursors of extreme precipitation events over southwest China during the rainy season. *Journal of Geophysical Research: Atmosphere*, *126*(13), e2021JD035134. https://doi.org/10.1029/2021JD035134

Park, I. H., & Min, S. K. (2017). Role of convective precipitation in the relationship between subdaily extreme precipitation and temperature. *Journal of Climate*, *30*(23), 9527–9537. https://doi.org/10.1175/jcli-d-17-0075.1

Pedregosa, F., Varoquaux, G., Gramfort, A., Michel, V., Thirion, B., Grisel, O., et al. (2011). Scikit-learn: Machine learning in Python. *Journal of Machine Learning Research*, *12*(85), 2825–2830. https://doi.org/10.5555/1953048.2078195

Pei, J., Wang, L., Xu, W., Kurz, D. J., Geng, J., Fang, H., et al. (2019). Recovered Tibetan antelope at risk again. *Science*, *366*(6462), 194. https://doi.org/10.1126/science.aaz2900

Pfahl, S., O'Gorman, P. A., & Fischer, E. M. (2017). Understanding the regional pattern of projected future changes in extreme precipitation. *Nature Climate Change*, *7*(6), 423–427. https://doi.org/10.1038/nclimate3287

Qian, C., Ye, Y., Zhang, W., & Zhou, T. (2022). Heavy rainfall event in mid-August 2020 in southwestern China: Contribution of anthropogenic forcings and atmospheric circulation. *Bulletin America Meteorology Social*, *103*(3), S111–S117. https://doi.org/10.1175/bams-d-21-0233.1

Qian, T., Zhao, P., Zhang, F., & Bao, X. (2015). Rainy-season precipitation over the Sichuan basin and adjacent regions in southwestern China. *Monthly Weather Review*, *143*(1), 383–394. https://doi.org/10.1175/mwr-d-13-00158.1

Sandvik, M. I., Sorteberg, A., & Rasmussen, R. (2018). Sensitivity of historical orographically enhanced extreme precipitation events to idealized temperature perturbations. *Climate Dynamics*, *50*(1), 143–157. https://doi.org/10.1007/s00382-017-3593-1

Shen, C., Li, G., & Dong, Y. (2022). Vertical structures associated with orographic precipitation during warm season in the Sichuan Basin and its surrounding areas at different altitudes from 8-year GPM DPR observations. *Remote Sensing*, *14*(17), 4222. https://doi.org/10.3390/rs14174222

Sun, G., Hu, Z., Ma, Y., Xie, Z., Sun, F., Wang, J., & Yang, S. (2021). Analysis of local land atmosphere coupling characteristics over Tibetan Plateau in the dry and rainy seasons using observational data and ERA5. *Science of the Total Environment*, *774*, 145138. https://doi.org/10.1016/j.scitotenv.2021.145138

Tang, S., Li, R., He, J., Wang, H., Fan, X., & Yao, S. (2020). Comparative evaluation of the GPM IMERG early, late, and final hourly precipitation products using the CMPA data over Sichuan Basin of China. *Water*, *12*(2), 554. https://doi.org/10.3390/w12020554

Tang, Y., Huang, A., Wu, P., Huang, D., Xue, D., & Wu, Y. (2021). Drivers of summer extreme precipitation events over East China. *Geophysical Research Letters*, *48*(11), e2021GL093670. https://doi.org/10.1029/2021GL093670

Tian, L., Jin, J., Wu, P., Niu, G. Y., & Zhao, C. (2020). High-resolution simulations of mean and extreme precipitation with WRF for the soil-erosive Loess Plateau. *Climate Dynamics*, *54*(7), 3489–3506. https://doi.org/10.1007/s00382-020-05178-6

Tian, L., Yao, T., MacClune, K., White, J. W. C., Schilla, A., Vaughn, B., et al. (2007). Stable isotop-ic variations in west China: A consideration of moisture sources. *Journal of Geophysical Research*, *112*(D10), D10112. https://doi.org/10.1029/2006JD007718

Trenberth, K. E. (1998). Atmospheric moisture residence times and cycling: Implications for rainfall rates and climate change. *Climate Change*, *39*(4), 667–694. https://doi.org/10.1023/A:1005319109110

Tuel, A., & Martius, O. (2022). Subseasonal temporal clustering of extreme precipitation in the northern hemisphere: Regionalization and physical drivers. *Journal of Climate*, *35*(11), 3537–3555. https://doi.org/10.1175/jcli-d-21-0562.1

Utsumi, N., Kim, H., Kanae, S., & Oki, T. (2016). Which weather systems are projected to cause future changes in mean and extreme precipitation in CMIP5 simulations? *Journal of Geophysical Research*, *121*(18), 10522–510537. https://doi.org/10.1002/2016jd024939

Utsumi, N., Kim, H., Kanae, S., & Oki, T. (2017). Relative contributions of weather systems to mean and extreme global precipitation. *Journal of Geophysical Research*, *122*(1), 152–167. https://doi.org/10.1002/2016jd025222

von Luxburg, U. (2007). A tutorial on spectral clustering. *Statistics and Computing*, *17*(4), 395–416. https://doi.org/10.1007/s11222-007-9033-z

Wei, W., Zhang, R., Wen, M., Rong, X., & Li, T. (2014). Impact of Indian summer monsoon on the South Asian High and its influence on summer rainfall over China. *Climate Dynamics*, *43*(5), 1257–1269. https://doi.org/10.1007/s00382-013-1938-y

Wu, G., Duan, A., Liu, Y., Mao, J., Ren, R., Bao, Q., et al. (2015). Tibetan Plateau climate dynamics: Recent research progress and outlook. *National Science Review*, *2*(1), 100–116. https://doi.org/10.1093/nsr/nwu045

Wu, M. G., & Luo, Y. L. (2019). Extreme hourly precipitation over China: Research progress from 2010 to 2019. *Torrential Rain and Disasters*, *38*(5), 502–514. http://www.byzh.org.cn/CN/abstract/abstract2606.shtml

Wu, Y., Huang, A., Huang, D., Chen, F., Yang, B., Zhou, Y., et al. (2018). Diurnal variations of summer precipitation over the regions east to Tibetan Plateau. *Climate Dynamics*, *51*(11), 4287–4307. https://doi.org/10.1007/s00382-017-4042-x

Xia, R., Luo, Y., Zhang, D. L., Li, M., Bao, X., & Sun, J. (2021). On the diurnal cycle of heavy rainfall over the Sichuan basin during 10–18 August 2020. *Advances in Atmospheric Sciences*, *38*(12), 2183–2200. https://doi.org/10.1007/s00376-021-1118-7

Xiao, C., Wu, P., Zhang, L., & Song, L. (2016). Robust increase in extreme summer rainfall intensity during the past four decades observed in China. *Scientific Reports*, *6*(1), 1–9. https://doi.org/10.1038/srep38506

Xie, Z., Du, Y., Zeng, Y., & Miao, Q. (2018). Classification of yearly extreme precipitation events and associated flood risk in the Yangtze-Huaihe River Valley. *Science China Earth Sciences*, *61*(9), 1341–1356. https://doi.org/10.1007/s11430-017-9212-8

Xu, H., Goldsmith, Y., Lan, J., Tan, L., Wang, X., Zhou, X., et al. (2020). Juxtaposition of western Pacific subtropical high on Asian Summer Monsoon shapes subtropical Ea-st Asian precipitation. *Geophysical Research Letters*, *47*(3), e2019GL084705. https://doi.org/10.1029/2019GL084705

Xu, X., Lu, C., Shi, X., & Gao, S. (2008). World water tower: An atmospheric perspective. *Geophysical Research Letters*, *35*(20), L20815. https://doi.org/10.1029/2008GL035867

Yang, M., Liu, G., Chen, T., Chen, Y., & Xia, C. (2020). Evaluation of GPM IMERG precipitation products with the point rain gauge records over Sichuan, China. *Atmospheric Research*, *246*, 105101. https://doi.org/10.1016/j.atmosres.2020.105101

Yao, T., Thompson, L., Yang, W., Yu, W., Gao, Y., Guo, X., et al. (2012). Different glacier status with atmospheric circulations in Tibetan Plateau and surroundings. *Nature Climate Change*, *2*(9), 663–667. https://doi.org/10.1038/nclimate1580

Ye, Y., & Qian, C. (2021). Conditional attribution of climate change and atmospheric circulation contributing to the record-breaking precipitation and temperature event of sum-mer 2020 in southern China. *Environmental Research Letters*, *16*(4), 044058. https://doi.org/10.1088/1748-9326/abeeaf

Zhang, Q., Zheng, Y., Singh, V. P., Luo, M., & Xie, Z. (2017). Summer extreme precipitation in eastern China: Mechanisms and impacts. *Journal of Geophysical Research*, *122*(5), 2766–2778. https://doi.org/10.1002/2016jd025913

Zhang, S., Wang, D., Qin, Z., Zheng, Y., & Guo, J. (2018). Assessment of the GPM and TRMM precipitation products using the rain gauge network over the Tibetan Plateau. *Journal of Meteorological Research*, *32*(2), 324–336. https://doi.org/10.1007/s13351-018-7067-0

Zhao, Y., Huang, A., Kan, M., Dong, X., Yu, X., Wu, Y., et al. (2020). Characteristics of hourly extreme precipitation along the Yangtze River Basin, China during warm season. *Scientific Reports*, *10*(1), 1–13. https://doi.org/10.1038/s41598-020-62535-5

Zheng, Y., Gong, Y., Chen, J., & Tian, F. (2019). Warm-season diurnal variations of total, stratiform, convective, and extreme hourly precipitation over central and eastern China. *Advances in Atmospheric Sciences*, *36*(2), 143–159. https://doi.org/10.1007/s00376-018-7307-3

Zhong, S., & Yang, X. Q. (2015). Ensemble simulations of the urban effect on a summer rainfall event in the Great Beijing Metropolitan Area. *Atmospheric Research*, *153*, 318–334. https://doi.org/10.1016/j.atmosres.2014.09.005

Zhu, L., Lü, X., Wang, J., Peng, P., Kasper, T., Daut, G., et al. (2015). Climate change on the Tibetan Plateau in response to shifting atmospheric circulation since the LGM. *Scientific Reports*, *5*(1), 1–8. https://doi.org/10.1038/srep13318

Zou, X., & Ren, F. (2015). Changes in regional heavy rainfall events in China during 1961–2012. *Advances in Atmospheric Sciences*, *32*(5), 704–714. https://doi.org/10.1007/s00376-014-4127-y